Radio Pulsars
ASP Conference Series, Vol. to be determined, 2003
M. Bailes, D. J. Nice, & S. E. Thorsett, eds.

Neutron Star Masses from Arecibo Timing Observations of Five Pulsar–White Dwarf Binary Systems

David J. Nice & Eric M. Splaver

Physics Department, Princeton University
Box 708, Princeton, NJ 08544 USA

Ingrid H. Stairs

Department of Physics and Astronomy, University of British Columbia
6224 Agricultural Road, Vancouver, BC V6T 1Z1, Canada

Abstract. We have detected relativistic and/or kinematic post-Keplerian parameters of no fewer than five pulsar–white dwarf binary systems in long-term timing observations at Arecibo. We discuss the resulting constraints on pulsar and companion masses. The general trend is that the pulsar mass measurements are compatible with the canonical value of $1.35\,M_\odot$, but in most cases somewhat higher masses are preferred.

1. Introduction

Evolutionary considerations suggest that pulsars in white dwarf–neutron star binaries might have masses higher than the canonical value of $1.35\,M_\odot$, perhaps due to extended, stable mass transfer. Here we report on observations of five pulsars in such binary systems. We have measured one or more post-Keplerian effects in each system, leading to constraints on the pulsar masses. (For a review of previous pulsar mass measurements, see Thorsett & Chakrabarty 1999.)

We observed the pulsars over several years with the post-upgrade Arecibo telescope. We used the Princeton Mark IV data acquisition system to perform baseband sampling, coherent dedispersion, pulse-synchronous folding, and timing (Stairs et al. 2000). Depending on the pulsar, we also used data collected at Green Bank (140 Foot telescope), Jodrell Bank, and/or Effelsberg, as well as data from the Arecibo Berkeley Pulsar Processor and the Princeton Mark III system (pre-upgrade Arecibo). Details will be given elsewhere.

2. Constraints on Pulsar and Companion Mass

2.1. Keplerian Mass Function

For each system, five Keplerian parameters are measured: orbital period, P_b; eccentricity, e; angle of periastron, ω; time of periastron passage, T_0; and projected semi-major axis, $x = (a_1 \sin i)/c$, where a_1 is the semi-major axis of the pulsar orbit, i is the orbital inclination angle, and c is the speed of light. These combine to form the mass function, $f_1 = (m_2 \sin i)^3 (m_1 + m_2)^{-2} = (2\pi/P_b)^2 x^3 / T_\odot$,

where $T_\odot = 4.925\,\mu$s is the solar mass in time units, and where m_1 and m_2 are the mass of the pulsar and its companion, respectively, in solar mass units. While i is unknown, the constraint $\sin i \leq 1$ leads to $m_1 < m_2^{3/2} f_1^{-1/2} - m_2$.

2.2. Relativistic Phenomena

Three relativistic phenomena constrain the system masses.

Precession of an orbit can be measured if eccentricity is sufficiently large. (For circular orbits, precession is completely covariant with orbital period.) The rate of apsidal advance is $\dot{\omega} = 3(P_b/2\pi)^{-5/3}(1-e^2)^{-1}T_\odot^{2/3}(m_1+m_2)^{2/3}$, so measurement of $\dot{\omega}$ yields total mass, $m_1 + m_2$.

Shapiro delay, the excess propagation time through the gravitational potential well of the secondary is, for small e, $\Delta t_s = -2\,m_2\,T_\odot \ln[1-\sin i \sin(\phi-\phi_0)]$, where ϕ is the orbital phase measured from the ascending node, ϕ_0. For edge-on orbits (large i), detection of Shapiro delay leads to measurement of m_2 and $\sin i$. For face-on orbits (small i), Shapiro delay is covariant with projected semi-major axis and cannot be detected; this non-detection can be used to exclude high-inclination, low-companion-mass orbits.

Orbital decay due to gravitational radiation causes P_b to change at a rate $\dot{P}_b = -(192\pi/5)(P_b/2\pi)^{-5/3}(1+\frac{73}{24}e^2+\frac{37}{96}e^4)(1-e^2)^{-7/2}\,T_\odot^{5/3}\,m_1\,m_2\,(m_1+m_2)^{-1/3}$. This can be measured for sufficiently small orbits (low P_b).

2.3. Kinematic $\dot{x}$

Motion of a binary system relative to the Sun induces a change in the inclination angle of the orbit, and hence a change in the projected semi-major axis, $\dot{x}/x = -\mu \cot i \sin\theta$, where μ is the (measured) proper motion and θ is the (*a priori* unknown) difference between the position angle of proper motion and the position angle of the ascending node (Kopeikin 1996; see also Nice, Splaver, & Stairs 2001). Measurement of $\dot{x}$ alone does not yield a value of i, but the constraint $|\sin\theta| \leq 1$ leads to $i < \tan^{-1}(\mu x/\dot{x})$, giving a firm upper limit on i.

2.4. Orbital Period–Core Mass relation.

Studies of low- and intermediate-mass binary evolution predict a nearly unique relation between P_b and m_2 in pulsar–helium white dwarf binaries (Podsiadlowski, Rappaport, & Pfahl 2002; Tauris & Savonije 1999; Rappaport et al. 1995). The $P_b - m_2$ relation may be used to constrain the system masses; alternatively, measured system masses may be used to test the evolution theory.

3. Timing Analysis and Results

Table 1 summarizes the post-Keplerian phenomena detected in each of five pulsar binaries. For each pulsar, we used TEMPO[1] to calculate the goodness-of-fit of timing solutions over a uniform grid of $\cos i$ and m_2 values. In each timing run, relativistic parameters appropriate to the given $\cos i$ and m_2 were calculated and

[1] http://pulsar.princeton.edu/tempo

Table 1. Pulsar Parameters and Post-Keplerian Detections

Pulsar	P_b	e	f_1	Post-Keplerian Parameters			
	(Days)		($M_\odot$)	$\dot{\omega}$	Shapiro	$\dot{P}_b$	$\dot{x}$
J0621+1002	8.32	0.002 457	0.0270	$\surd$	limit		
J0751+1807	0.26	0.000 003	0.0010		maybe?	soon!	
J1713+0747	67.83	0.000 075	0.0079		$\surd$		$\surd$
B1855+09	12.33	0.000 022	0.0056		$\surd$		
J2019+2425	76.51	0.000 111	0.0107		limit		$\surd$

held constant, while all other parameters were allowed to vary. The gray regions in figures 1 and 2 show combinations of $\cos i$ and m_2 that gave acceptable fits at the 68% and 95% confidence levels (inner and outer contours).[2]

For each pulsar (except J2019+2425), the grids of timing runs were used to calculate the probability distribution function (pdf) for the underlying value of m_1. Briefly, the $\Delta\chi^2$ value from each grid point was translated into a probability and, after suitable normalization, the probabilities associated with a given range of m_1 were summed, resulting in a pdf for m_1. The limits on m_1 from each pdf are given in table 2. See Splaver et al. 2002 for more details on this procedure.

3.1. PSR J0621+1002

The relatively high eccentricity of this system (still only $e = 0.0025$!) is sufficient to break the covariance between P_b and $\dot{\omega}$ in the timing fit. We measure $\dot{\omega} = 0.0116 \pm 0.0008^\circ\,\mathrm{yr}^{-1}$ (1σ), yielding $m_1 + m_2 = 2.8 \pm 0.3\,M_\odot$. This corresponds to the strip between dashed lines in figure 1a. We do not detect Shapiro delay, so orbits with high i are excluded, closing off the gray region towards the lower right portion of figure 1a. The low eccentricity of the system, along with the lack of a detectable optical companion, provides strong evidence the companion is a white dwarf, so $m_2 < 1.4\,M_\odot$. As figures 1a and 1b show, the orbit is relatively close to face on, and the pulsar and companion masses are relatively high. Further discussion can be found in Splaver et al. 2002.

3.2. PSR J0751+1807

This binary has a very short orbital period, only 6.3 hours. The relativistic decay rate is expected to be around $\dot{P}_b \sim -4 \times 10^{-14}$, depending on the system masses (see figure 2a for representative calculations). The current data give $\dot{P}_b = (2 \pm 8) \times 10^{-14}$, tantalizingly close to the expected value. Results of a full relativistic timing analysis (figure 2a) show that higher values of i are preferred, implying a marginal detection of Shapiro delay. The pulsar mass is not yet measured, though there is a strong upper limit $m_2 < 2.07\,M_\odot$.

We anticipate that future observations will substantially reduce the uncertainty of $\dot{P}_b$. (For a pulsar observed uniformly over time span t, the uncertainty of $\dot{P}_b$ scales as $t^{-2.5}$.) This will be the first detection of relativistic decay outside of double-neutron-star binaries.

[2]For J0621+1002, the contours are at 39% and 86% confidence levels.

Table 2. Mass Measurements from Timing Analysis

Pulsar	Pulsar Mass, m_1 ($M_\odot$)		
	Best Value	68% confidence	95% confidence
J0621+1002	1.70	1.41−2.02	1.07−2.29
J0751+1807	0.55	0.19−1.25	0.02−2.07
J1713+0747	1.85	1.49−2.26	1.23−2.83
B1855+09	1.57	1.46−1.69	1.37−1.82

3.3. PSR J1713+0747

This pulsar in a wide binary has a strong, sharp pulse, allowing us to achieve timing precision of 200−400 ns in a single observation. Camilo, Foster, & Wolszczan (1994) first reported the detection of Shapiro delay. Our data give substantially improved constraints on the system masses and inclination (figure 2b). The timing data still allow a wide range of pulsar masses (table 2), but the overlap between parameters allowed by the timing data and the range of m_2 predicted by the P_b-m_2 relation of Tauris & Savonije (1999) gives a tighter constraint on m_1, 1.46−1.61 $M_\odot$ (figure 2b). (The binary evolution tracks of Podsiadlowski et al. 2002 give very similar predictions.)

3.4. PSR B1855+09

Our new data only modestly augments that of Kaspi, Taylor, & Ryba (1994) and earlier work. Shapiro delay gives tight constraints on m_2 and i (figure 2c), which are in excellent agreement with the P_b-m_2 relation.

3.5. PSR J2019+2425

No relativistic effects are detected. The observed $\dot{x}/x = 1.3 \pm 0.2 \times 10^{-15}\,\mathrm{s}^{-1}$ constrains $i < 72°$. Shapiro delay is not detected, also constraining the system away from high i (figure 2d). Little can be said about the system masses from timing alone. However, if m_2 is within the range allowed the P_b-m_2 relation (horizontal strip in figure 2d), the neutron star mass must be $m_1 < 1.51\,M_\odot$. Further analysis of this system is given in Nice, Splaver, & Stairs 2001.

4. Conclusion

Table 2 shows substantial constraints on neutron star mass m_1 from timing alone for three of the five pulsars, J0621+1002, J1713+0747, and B1855+09. In each case, the 68% confidence limits on m_1 are above the canonical neutron star mass of 1.35 $M_\odot$, although the 95% ranges all encompass this value. PSR J0437−4715 is similar, with $m_1 = 1.58 \pm 0.18\,M_\odot$ (van Straten et al. 2001). The evidence is mounting that some pulsars are heavier than 1.35 $M_\odot$, though this cannot yet be considered conclusive. The P_b-m_2 relation is in good agreement with the timing data and with the relatively high pulsar masses.

The most exciting prospect for the future is PSR J0751+1807. Although its mass is only weakly constrained, especially on the lower end, great advances will be made as the decay of this pulsar's orbit is measured in coming years.

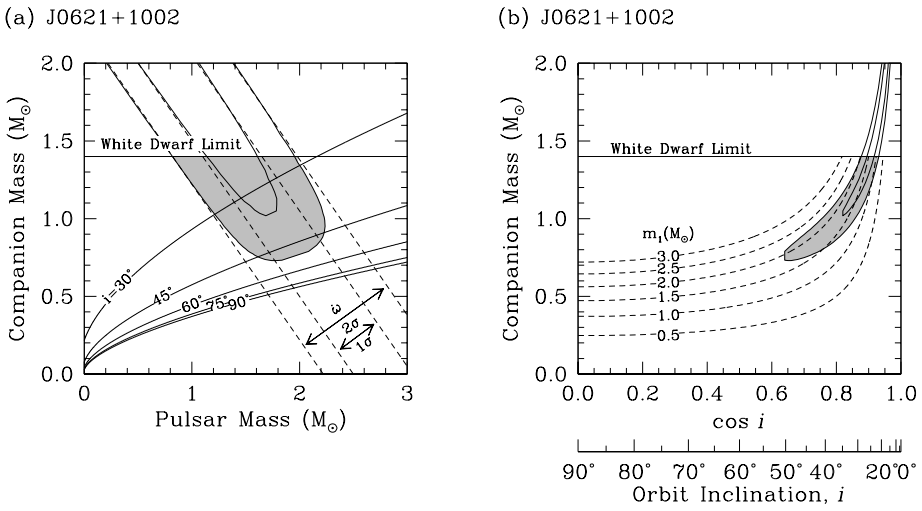

Figure 1. Constraints on PSR J0621+1002 parameters. See text.

Acknowledgments. Portions of this work are collaborations with Zaven Arzoumanian, Don Backer, Fernando Camilo, Michael Kramer, Andrea Lommen, Oliver Löhmer, and Andrew Lyne. We are indebted to Joe Taylor and Steve Thorsett for development work on the Princeton Mark IV system and to Kiriaki Xilouris and Dunc Lorimer for efforts in advancing pulsar astronomy on the post-upgrade Arecibo telescope. The Arecibo Observatory is operated by Cornell University under a cooperative agreement with the National Science Foundation. Pulsar research at Princeton University is supported by the NSF. IHS is supported by an NSERC UFA and Discovery Grant.

References

Camilo, F., Foster, R. S., & Wolszczan, A. 1994, ApJ, 437, 39

Kaspi, V. M., Taylor, J. H., & Ryba, M. F. 1994, ApJ, 428, 713

Kopeikin, S. M. 1996, ApJ, 467, L93

Nice, D. J., Splaver, E. M., & Stairs, I. H. 2001, ApJ, 549, 516

Podsiadlowski, P., Rappaport, S., & Pfahl, E. D. 2002 ApJ, 565, 1107

Rappaport, S., Podsiadlowski, P., Joss, P. C., DiStefano, R., & Han, Z. 1995, MNRAS, 273, 731

Splaver, E. M., Nice, D. J., Arzoumanian, Z., Camilo, F., Lyne, A. G., & Stairs, I. H. 2002, ApJ, in press, astro-ph/0208281

Stairs, I. H., Splaver, E. M., Thorsett, S. E., Nice, D. J. & Taylor, J. H. 2000, MNRAS, 314, 459

Tauris, T. M. & Savonije, G. J. 1999, A&A, 350, 928

Thorsett, S. E. & Chakrabarty, D. 1999, ApJ, 512, 288

van Straten, W., Bailes, M., Britton, M., Kulkarni, S. R., Anderson, S. B., Manchester, R. N., & Sarkissian, J. 2001, Nature, 412, 158

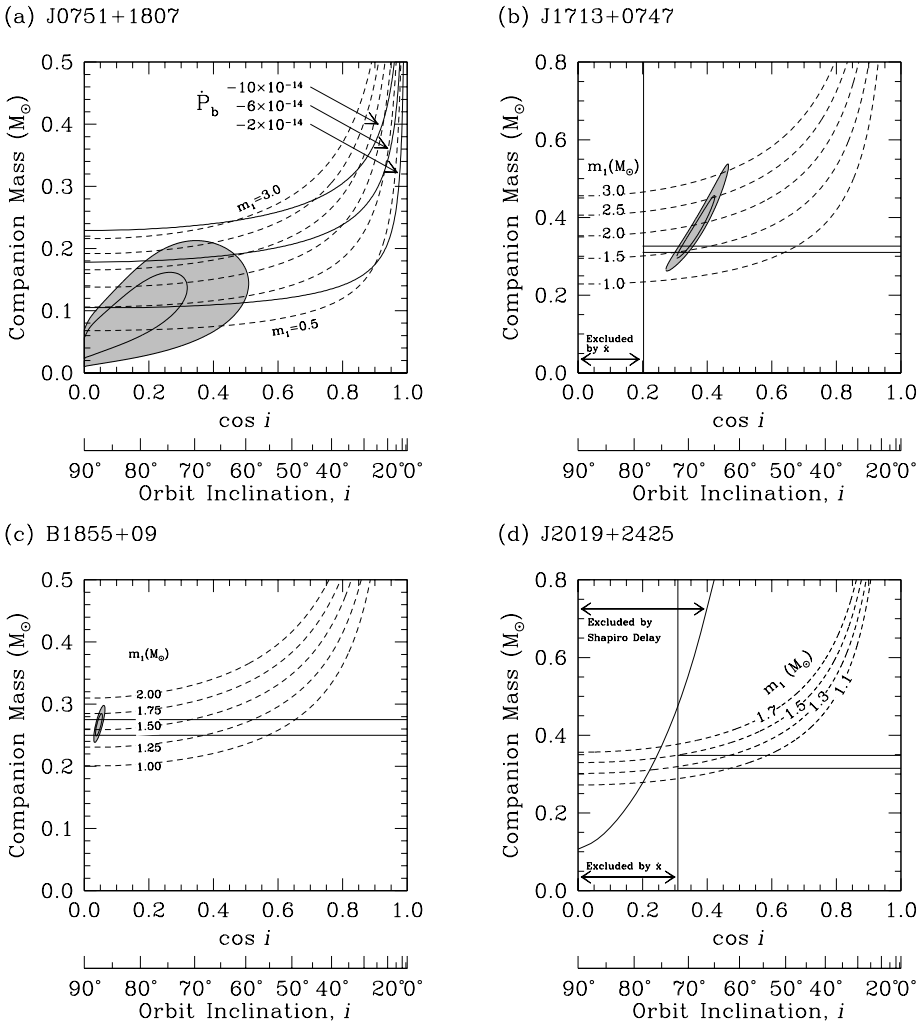

Figure 2. Constraints on $\cos i$ and m_2. Dashed lines show representative values of m_1. Gray regions denote the area allowed by the data. When present, a vertical line indicates the largest i allowed by a measured $\dot{x}$, and horizontal lines indicate the range of m_2 predicted by the $P_b - m_2$ relation. (a) PSR J0751+1807. Solid lines show representative values of $\dot{P}_b$. (b) PSR J1713+0747. (c) PSR B1855+09. (d) PSR J2019+2425. The curved solid line delimits the region in the upper left excluded by the non-detection of Shapiro delay.